THE JOURNAL OF PHYSICAL CHEMISTRY C

Article

pubs.acs.org/JPCC

Photomagnetic Carbon Nanotubes at Ambient Conditions

Wei Shen Lin,[†] Yueh-Hua Han,[†] Ting-Yu Chang,[†] Chong Mou Wang,*[,†] Cheng-Hsun-Tony Chang,[‡] and Jyh-Shen Tsay*[,‡]

[†]Department of Chemistry and [‡]Department of Physics, National Taiwan Normal University, Taipei 116, Taiwan

Supporting Information

ABSTRACT: Bis(2,2-bipyridine)-5-amino-1,10-phenanthroline ruthenium(II) ($Ru(bpy)_2(phen\text{-}NH_2)^{2+}$), an MLCT complex, has a long-lived triplet state in water (λ_{ex}: 473 nm; λ_{em}: 620 nm; τ = 615 ns; Φ = 1 relative to that of $Ru(bpy)_3^{2+}$) and a structure analogous to $Ru(bpy)_3^{2+}$. When $Ru(bpy)_2(phen\text{-}NH_2)^{2+}$ was subjected to diazotization in the presence of carbon nanotubes (CNTs), it formed nanodots on the CNTs, rendering the resulting tubes (Ru@CNT) capable of transducing photo stimuli (473 nm) into electricity and magnetism at ambient conditions. The increased functionality was highly reproducible, as evidenced by conductive-mode AFM, vibrating sample magnetometry (VSM), and AC susceptibility analysis. The local magnetism probing of the Ru@CNT with magnetic-mode AFM techniques (MFM) indicated that the magnetism originated from the unpaired electrons formed on the photoexcited nanodots. The resulting phase shift behaved as a function of the luminous power and the voltage (V_b) of the electrical bias applied to the Ru@CNT. The V_b dependence deviated from the expected quadratic correlation, confirming that the formation of the photoinduced charge separation state at the nanodots is responsible for the photomagnetism. The Ru@CNT tubes showed mobility toward external magnets (65 G) when floating on water and under 473 nm illumination. The Ru@CNT thus appears to be a multifunctional material that might be useful in spintronics.

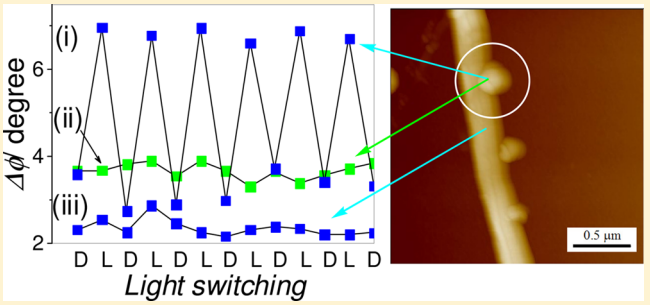

1. INTRODUCTION

The optical control of physical properties and the development of new materials with increased functionality are subjects of intensive research in the area of materials science.[1,2] Carbon nanotubes (CNTs) represent such a multifunctional material, featuring high chemical stability, excellent mechanical strength,[3] and diverse electronic properties that depend on their helicity and size[4] and can be manipulated by an external electromagnetic field.[5] In contrast to their electronic characteristics, intrinsic CNTs are diamagnetic at room temperature.[6] Although this conclusion remains the subject of some debate,[7] examples of applications of intrinsic CNTs in magnetism-related applications at ambient conditions are rare.[8,9] CNTs can be magnetized by the presence of ferromagnetic nanocrystals,[10] by the creation of a ferromagnetic surface,[11] or through chemical modification.[12] Various magnetic CNTs have been prepared as of this writing, and the products have the potential for use in many fields.[13] Despite this, preparing photomagnetic CNTs continues to remain a challenge.[14]

Photomagnetism dates back to 1967, when silicon-doped yttrium iron garnet was reported to develop magnetocrystalline anisotropy on exposure to IR irradiation.[15] Since that report, a handful of spin-crossover compounds have been characterized,[16] but most show short lifetimes for the photoinduced spin states at ambient temperature. In 2002, Shimamoto et al. observed that the electronic state of $Na_{0.68}Co_{1.20}[Fe(CN)_6]\cdot 3.7H_2O$ could be converted from $Fe^{II}(S = 0)$-CN-$Co^{III}(S = 0)$ to $Fe^{III}(S = 1/2)$-CN-$Co^{II}(S = 3/2)$ under laser-pulse irradiation at room temperature.[17] Liu et al. supported the observation, showing that the reversible valence tautomeric conversion in $Na_{0.36}Co_{1.32}Fe(CN)_{6.5}\cdot 6H_2O$ could be induced by a single-shot laser pulse (duration of 8 ns) above 200 K in a thermal hysteresis loop due to a cooperative interaction among the local photoexcited sites.[18] By monitoring the photoexcited heptanuclear complex $[Mo^{IV}(CN)_2(CNCuL)_6]^{8+}$ (L: tris(2-aminoethyl)amine) at low temperature, Herrera et al. reported on the formation of a high-spin molecule with ferromagnetic interaction between the spin carriers.[19] In 2005, Kimel employed circularly polarized femtosecond laser pulses to control the spin dynamics in $DyFeO_3$ at low temperature, offering prospects for applications of ultrafast lasers in magnetic devices.[20] According to the progress of photomagnetic materials, Létard suggested a guideline for the rational design of materials with long-lived photomagnetic lifetimes at room temperature.[21] In 2008, Cobo et al. isolated $\{Fe^{II}(pyrazine)[Pt(CN)_4]\}$ and reported that the crystals exhibited a thermal spin transition at around room temperature, which was accompanied by a 14 K wide hysteresis loop. Within the thermal hysteresis region a complete bidirectional photoconversion between the high-spin and low-spin phases occurred when the sample was irradiated with a short single laser pulse (4 ns, 532 nm).[22] Bozdag et al. also observed reversible

Received: May 11, 2015
Revised: August 15, 2015
Published: August 17, 2015

DOI: 10.1021/acs.jpcc.5b04532
J. Phys. Chem. C 2015, 119, 20673−20680

photoinduced magnetic phenomena for a V−Cr prussian blue analogue. When illuminated with UV light (350 nm) at low temperatures (10 K), the magnet exhibited a change in magnetization due to structural distortion, and the photo-excited magnetic state completely recovered back to the ground state via thermal relaxation or partially recovered when illuminated with green light (514 nm).[23] Inspired by the room-temperature photoinduced electron transfer occurring in prussian blue analogues, researchers agree that the use of light can have future applications in the elaboration of molecular memories and switching devices.[24] From theoretical aspects, charge-transfer complexes are potential candidates for use in photomagnetic applications at ambient conditions, because many metal complexes possess a relatively long lifetime that is associated with a metal-to-ligand charge transfer (^{3}MLCT) excited state, and the ability to act as an electron acceptor or donor.[25] The findings reported herein show that when CNTs are surface-bonded with bis(2,2-bipyridine)-5-amino-1,10-phenanthroline ruthenium(II) ($Ru(bpy)_2(phen\text{-}NH_2)^{2+}$),[26] a long-lived ^{3}MLCT molecule, the resulting tubes exhibit magnetism when exposed to visible light at room temperature. This photomagnetism is highly reproducible, revealing the potential for use in spintronics research.[27]

Scheme 1. Schematic Illustration for the Preparation of the Ru@CNT

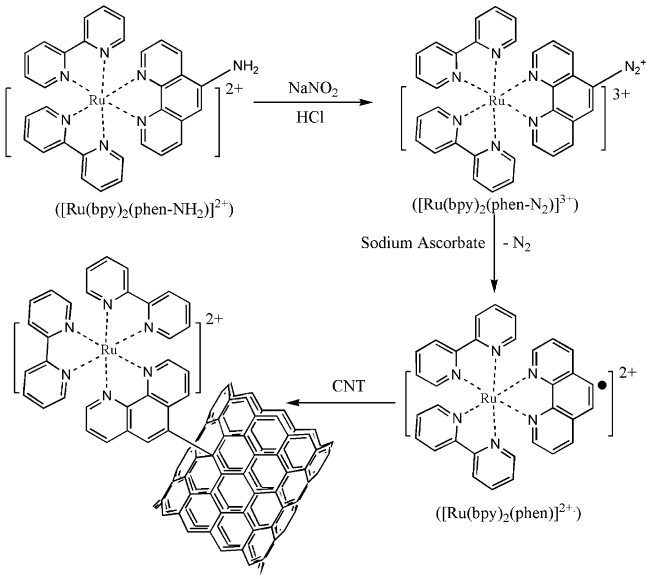

2. EXPERIMENTAL SECTION

2.1. Chemicals. Bis(2,2-bipyridine) ruthenium(II) dichloride ($Ru(bpy)_2{\cdot}2Cl$), 5-amino-1,10-phenanthroline (phen-NH_2), sodium nitrite ($NaNO_2$), sodium ascorbate, and ammonium hexafluorophosphate (NH_4PF_6) were purchased from Sigma-Aldrich. Multiwalled carbon nanotube (purity > 99%; length, 5−15 μm) was supplied by Golden Innovation Business Corp. Ltd., Taiwan. All chemicals were used as received without further purification. $Ru(bpy)_2(phen\text{-}NH_2){\cdot}2PF_6$ was synthesized according to a procedure described in the literature.[26] Typically, 1.1 mmol of phen-NH_2 was dissolved with 1.0 mmol $Ru(bpy)_2{\cdot}2Cl$ in 100 mL of a hot ethanol−water mixture (v/v 1:1). The product was then subjected to anion exchange with NH_4PF_6 (5 mmol in 10 mL of H_2O). The crystal structure and the transient emission spectra of the final product are provided in Figures S1 and S2 (Supporting Information), respectively. The $Ru(bpy)_2(phen\text{-}NH_2)^{2+}$-modified carbon tubes (Ru@CNT) were prepared by reacting $Ru(bpy)_2(phen\text{-}NH_2){\cdot}2PF_6$ with multiwalled CNTs in HCl solutions via the processes schematically illustrated in Scheme 1.

Typically, $Ru(bpy)_2(phen\text{-}NH_2){\cdot}2PF_6$ (0.1 mmol) and CNTs (50 mg) were allowed to react in 50 mL of HCl (1 M) in the presence of $NaNO_2$ and sodium ascorbate (0.1 mmol each) at 80 °C under a N_2 atmosphere for 4 h. TEM analysis (Figure S3) showed that the $Ru(bpy)_2(phen\text{-}NH_2)^{2+}$-derived radicals formed small seeds on the tubes at the early stage of the reaction, gradually transformed into beads with an average size of 100 nm after 1 h, and grew to be ∼500 nm after 4 h. The representative UV−vis absorption spectra of the Ru@CNTs are provided in Figure S4.

2.2. Apparatus. A potentiostat (PAR 283, EG&G) was used to record cyclic voltammograms (CVs). Unless otherwise specified, all experiments were carried out under nitrogen in a one-compartment cell equipped with a Pt working electrode (1 mm in diameter), a Pt counter electrode, and an SCE reference electrode. UV−vis absorption spectra were recorded with an HP 8453 UV−visible spectrometer, and emission spectra were measured with an Aminco-Bowman luminescence spectrophotometer (series 2). The transient emission spectra of $Ru(bpy)_2(phen\text{-}NH_2)^{2+}$ were recorded with a luminescence spectrometer (FLS 920-t, Edinburgh Instruments Ltd., U.K.). Samples (ca. 0.3 g L^{-1}) were all degassed prior to the laser experiments. Luminescence decay kinetics were deconvoluted from the instrumental response function to give single exponential decays. Raman spectra were recorded using Dilor 800 XY spectrometer under ambient conditions. For laser excitation, we used 514.5 nm (2.41 eV) line from Ar^+. Transmission electron microscopic analysis (TEM) was carried out with a JEOL JEM-2200FS transmission electron microscope operating at 100 kV. Scanning electron microscopic (SEM) analyses were performed on a JEOL 6510 scanning electron microscope operating at 10 kV. An atomic force microscope (AFM, Nanoscope III E, Digital Instrument Corp.) with a 10 μm scanner was employed for morphology analysis. The AFM was also used in conjunction with a home-built preamplifier (sensitivity, 1 nA/V; operational range, 1 pA ∼ 10 nA) for current−voltage (I−V curves) and conductive-mode AFM measurements. The conductivity of the bare CNTs and the Ru@CNTs was determined by placing them between two ITO electrodes separated by a 1 μm wide dielectric groove (1 μm deep) fabricated by photo etching on ITO conductive glass (0.2 × 0.2 cm^2, 20 Ω/square, Delta Technologies, Figure S5). One side of the ITO served as the source and the other as the drain. An ohmic contact was made by applying silver paint (Alfa). Phase images were also recorded with the AFM by interleaving the topographic scan with the lift-mode scan. The magnetized tip scanned the sample as a free-standing cantilever at a constant lift height above the topographic height of the sample at each point. Magnetization versus magnetic field (M−H) curves were measured using a vibrating sample magnetometer (Lake Shore 7400 series) at a head drive frequency of 82 Hz. The alternative-current (AC) magnetic susceptibility (χ_{AC}) was examined using a susceptibility analyzer (XacQuan, MagQu) in a driving frequency range between 50 and 25 kHz.

3. RESULTS AND DISCUSSION

$Ru(bpy)_2(phen\text{-}NH_2)^{2+}$ is a metal-to-ligand charge-transfer complex. Its triplet excited state persists for 615 ns in terms

DOI: 10.1021/acs.jpcc.5b04532
J. Phys. Chem. C 2015, 119, 20673−20680

of the lifetime (τ) in water, and the quantum yield (Φ) is 1 relative to that of $Ru(bpy)_3^{2+}$ (Table S1). $Ru(bpy)_2(phen\text{-}NH_2)^{2+}$ can also be converted into a radical after diazotization in acidic $NaNO_2$ solutions.[28] Figure 1 shows that when $Ru(bpy)_2(phen\text{-}NH_2)^{2+}$ reacts with CNTs in an acidic $NaNO_2$ solution, submicrodots (denoted as Ru(II)-$phen^{2+}$, ~500 nm in diameter) are produced on the CNTs.

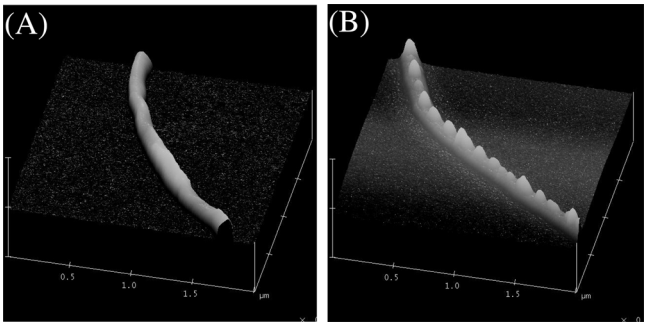

Figure 1. AFM images of a CNT before (A) and after (B) modified with $Ru(bpy)_2(phen\text{-}NH_2)^{2+}$ in an acidic $NaNO_2$ solution.

The formation of the nanodots leads to a sharp contrast in Ru (relative to the background Si) between the areas that contain attached nanodots and areas where they are absent, as revealed by energy dispersive X-ray analysis (Figure 2, curves

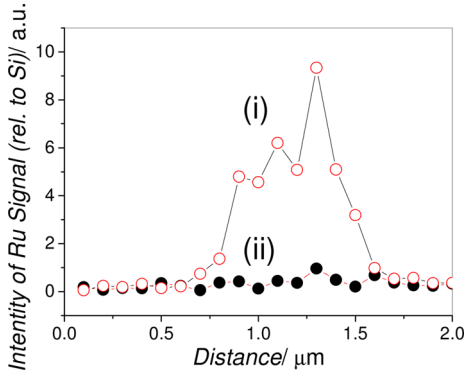

Figure 2. Distributions of Ru across the surface of the Ru@CNT deposited with (i) and without the nanodots (ii).

(i) and (ii)), and this perturbs the Raman spectra of the host (Figure 3), in which the *D* band (1340 cm^{-1}) is clearly enhanced at the expense of the *G* band (1576 cm^{-1}) and the second-order harmonic *G′* band (2694 cm^{-1}), similar to the reports of CNTs that are produced during their functionalization with aromatic diazonium salts.[29] These results indicate that the hybridization of some of the carbon atoms on the surface of the host have changed from sp^2 to sp^3 due to the coupling of the $Ru(bpy)_2(phen)^{2+\bullet}$ radical.[30] Since the radical can also undergo a self-coupling reaction by anchoring itself to the two bipyridines on the other radicals,[31] multilayer deposition can occur, thus, leading to the formation of the nanodots. The $Ru(bpy)_2(phen\text{-}NH_2)^{2+}$ derivatives can also form nanodots on graphite (highly oriented pyrolyzed graphite, Figure S6). The resulting nanoparticles are uniformly deposited on the substrate, which supports the mechanism proposed in Scheme 1.

The CNTs with adsorbed Ru(II)-$phen^{2+}$ (Ru@CNT) absorb weakly at 285, 433, and 456 nm (Figure S4), and no

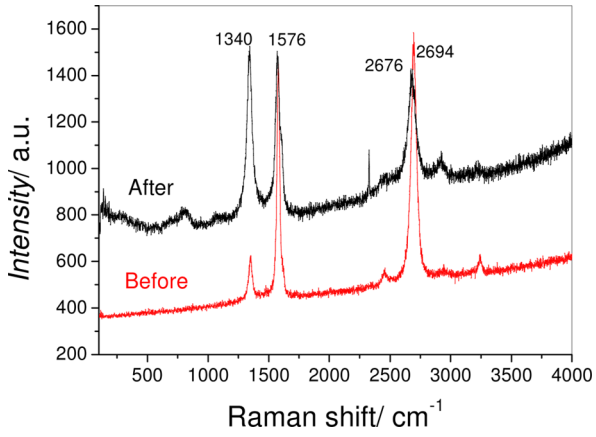

Figure 3. Raman spectra of CNTs before and after modification with $Ru(bpy)_2(phen\text{-}NH_2)^{2+}$.

photoresponses were observed when excited at these wavelengths, which is in contrast to $Ru(bpy)_2(phen\text{-}NH_2)^{2+}$ and its diazonium derivatives, $Ru(bpy)_2(phen\text{-}N_2)^{3+}$ and $Ru(bpy)_2(phen)^{2+}$. The lack of a photoresponse could result from a limited absorptivity for the excitation light, the quenching of emission by surface impurities/defects on the host, and an improper orientation toward the host surface.[32] However, based on energy-gap theory[33] and literature reports on CNTs[34] and complexes of ruthenium and other late transition metals,[35] we conclude that it more likely is due to nonradiation relaxation, because the CNT host can be regarded as an extension of the phenanthroline moiety. The increased distance between the electron donor and acceptor lowers the triplet state, but it also increases the probability of vibrational matching between the luminescent state and S_0. The expected luminescence may therefore be deactivated radiationlessly.[36] The radiationless decay supports the conclusion that the $Ru(bpy)_2(phen\text{-}NH_2)^{2+}$-derived radical had been covalently attached to the CNT host and, therefore, suggests that the nanodots are able to intercommunicate with their host via photoinduced electron transfer.[37]

As shown in Figure 4, when the Ru@CNT is positioned between two conductive ITO electrodes (Figure S5), significant amounts of electric current flow are observed to flow between the electrodes if the tube is illuminated at 473 nm. The onset potentials are approximately ±0.5 V, which can be attributed to the energy needed for the photoinduced charges to migrate

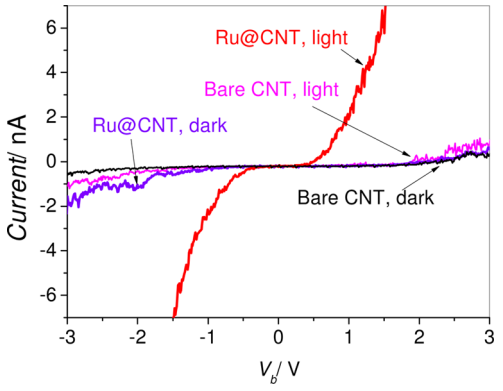

Figure 4. Current−voltage curves recorded with a single CNT and Ru@CNT in the dark and under illumination (473 nm, 27 mW).

DOI: 10.1021/acs.jpcc.5b04532
J. Phys. Chem. C 2015, 119, 20673−20680

across the Ru(II)-phen^{2+}|CNT junction. In this experiment, the electrical signals were monitored with a conductive-mode AFM tip in conjunction with one of the ITO electrodes, and a bias voltage (V_b, against the grounded tip) was applied through the other. In contrast, the bare CNT lacks such a characteristic within ±2 V in the dark or under illumination. The difference indicates that the Ru(II)-phen^{2+} dots are an effective photosensitizer, and the CNT host, an intrinsic semiconductor with a bandgap wider than 2 eV (E_g > 2 eV). Based on the 0−0 transition energy (E_{0-0}) and the CV curves of Ru(bpy)$_2$(phen-NH$_2$)$^{2+}$ (Figure S7) and assuming that the Ru(II)-phen^{2+} and its precursor share similar energetics:

$$\text{Ru(II)-phen}^{2+} + h\nu \rightarrow \text{Ru(II)-phen}^{2+*} \quad E_{0-0} = 2.27 \text{ eV} \tag{1}$$

$$\text{Ru(II)-phen}^{3+} + e^- \rightarrow \text{Ru(II)-phen}^{2+}$$
$$E_1^{o'} = 1.27 \text{ V vs SCE} \tag{2}$$

$$\text{Ru(II)-phen}^{2+} + e^- \rightarrow \text{Ru(II)-phen}^{+}$$
$$E_2^{o'} = -1.25 \text{ V vs SCE} \tag{3}$$

$$\text{Ru(II)-phen}^{+} + e^- \rightarrow \text{Ru(II)-phen}$$
$$E_3^{o'} = -1.43 \text{ V vs SCE} \tag{4}$$

$$\text{Ru(II)-phen} + e^- \rightarrow \text{Ru(II)-phen}^{-}$$
$$E_4^{o'} = -1.70 \text{ V vs SCE} \tag{5}$$

we estimate the formal potentials of the Ru(II)-phen$^{2+*/3+}$ and Ru(II)-phen$^{2+*/+}$ states to be −1.0 and 1.0 V versus SCE, respectively. Considering the onset potentials shown in Figure 4, we propose that they reside 0.5 eV below the conduction band edge and above the valence band edge of the host, as illustrated in Scheme 2. The photoresponses are highly

Scheme 2. Schematic Illustration for the Energetics of the Ru@CNT under Photoexcitation

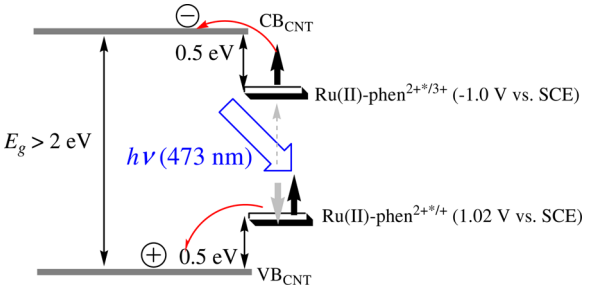

reproducible and behave as a function of the luminous power (Figure 5A). Although the minimum power for the 473 nm optical stimulus to be sensed by a single Ru@CNT at V_b = 1.0 V is around 11 mW (Figure 5B), the photosensitivity represents the first demonstration of a CNT-based transistor[38] in optical rectification.

Besides the functionality in optical rectification, the photoexcited Ru@CNT also exhibits magnetism at ambient conditions; representative results are shown in Figure 6. In the dark, the magnetic susceptibility (χ_{AC}) of the Ru@CNT increases slightly with a decrease in frequency; however, it is greatly enhanced when the analyte is exposed to 473 nm light (27 mW). Traces of ferromagnetic contaminants in the tube, such as iron, are likely to be the contributors to the dark magnetism. Some ruthenium debris produced as the result of decomposition of Ru(bpy)$_2$(phen-NH$_2$)$^{2+}$ during diazotization might also contribute, since nanosized nonmagnetic materials can also exhibit magnetic ordering.[39−43] Nevertheless, powdered Fe, Fe_3O_4, and Ru, as well as the bare CNTs, exhibited no appreciable photoresponses under similar conditions. The optimal resonance frequency for the illuminated Ru@CNT occurs near 2000 Hz,[44] where the corresponding spin sensitivity is ∼29.0 emu/g or about 15× the susceptibility in the dark. The ratio remained at ∼5, with the frequency being decreased to 100 Hz, highlighting that the Ru@CNT is a photomagnet. VSM experiments confirm the photomagnetism (Figure 7A). The Ru@CNT tubes show weak magnetism in the dark; however, the strength is enhanced when the tubes are exposed to 473 nm illumination, leading to a linear correlation between the net magnetization (ΔM) and the applied field (Figure 7B). We also attempted to determine the hysteresis for the tube using more sensitive techniques such as SQUID for comparison. Due to the limitations of the instrumental setup for simultaneous illumination, this was not possible. Despite this, the photoilluminated Ru@CNTs exhibited measurable mobility toward external magnets (65 G) while the tubes were floating on water (video provided in Supporting Information). The average velocity was estimated to be 0.24 mm/min. In contrast, the bare CNTs remained unmoved under similar conditions, indicating that the Ru@CNTs are a photomagnetic material, and the Ru(II)-phen^{2+} nanodots are responsible for the photomagnetism.

A local magnetism probing of the Ru@CNT with the magnetic field-mode AFM (MFM) indicates that the photomagnetic functionality arises from the photoexcited nanodots. As shown in Figure 8, when the nanodot designated with a circle is illuminated at 473 nm (27 mW; curve (i)), it strongly disturbs the oscillation of the MFM tip atop it. The perturbation effect is highly reproducible, but diminishes if the excitation is switched to 532 nm (curve (ii)) or if the tip is moved to an area free of Ru(II)-phen^{2+}, such as being 0.3 μm away from the nanodot (curve (iii)). Here, L and D denote on and off light; $\Delta\phi$ represents the shift in the cantilever's phase of oscillation relative to the piezo drive caused by the analyte, recorded at a constant lift height (h), 8 nm above the sample.

For the phase-shift measurements, we first determined the optimum lift height for the magnetized tip. By varying h from 2 to 50 nm and subtracting the background signals (ITO) from those resulting from the nanodots on the Ru@CNT such as that shown in the inset in Figure 9, we observed that the net phase shift ($\delta(\Delta\phi) = \Delta\phi_{dot} - \Delta\phi_{ITO}$) reached the maximum value when $h \rightarrow 8$ nm. Accordingly, we set the lift height to a constant 8 nm for all the MFM measurements in this work.

The phase shift observed under 473 nm illumination increases linearly with the luminous power when the tube is biased at a constant voltage (V_b = 3 V, Figure S8) or with the voltage if the luminosity is fixed (27 mW, Figure 10). The voltage dependence, however, diminishes when the light source is removed or replaced by a 532 nm laser, consistent with the excitation spectra of Ru(bpy)$_2$(phen-NH$_2$)$^{2+}$ (Figure S2). We also attempted to measure the phase shift at low temperature for comparison. Due to the limitations of the AFM stage for cooling, the attempt was not successful.

In theory, the phase shift of a magnetized tip depends on the gradient of the local magnetostatic force, $\partial F^M/\partial h$, and the electric field between the tip and the analyte:[45]

DOI: 10.1021/acs.jpcc.5b04532
J. Phys. Chem. C 2015, 119, 20673−20680

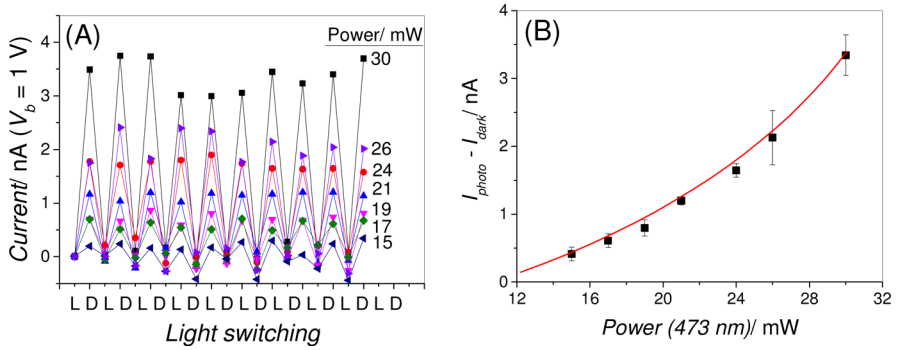

Figure 5. (A) Photoresponses of a single Ru@CNT to the 473 nm stimuli (13−30 mW) monitored at V_b = 1 V. (B) Correlation between the net photocurrent and the power of the light source.

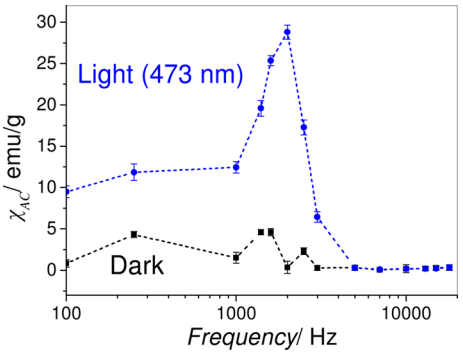

Figure 6. Magnetic susceptibility (χ_{AC}) of the Ru@CNT recorded under illumination (473 nm) and in the dark.

$$\Delta\phi \approx -(Q/k)(\partial F^{M}/\partial h) + k_{m}(\partial F^{E}/\partial h) \quad (6)$$

$$\partial F^{E}/\partial h = -(V_{b}^{2}/2)(\partial^{2}C/\partial h^{2}) \quad (7)$$

Here, Q stands for the proportionality constant; k, the spring constant of the cantilever; h, the distance between the tip and the analyte, equivalent to the lift height; k_m, a function of the effective magnetic moments of the analyte and tip; F^E, electric force; and, C, the tip-to-sample capacitance. The results presented in Figure 10 indicate that the magnetic moment (or k_m) of the nanodot ≠ 0 when the 473 nm light is on. The data, however, deviates from the V_b^2 dependence predicted by eq 7. The discrepancy could result from a nonconstant C, decreasing with V_b due to capacity saturation caused by the increased number of photoinduced charges as a result of the increased bias, or from a V_b-dependent k_m. We plotted the

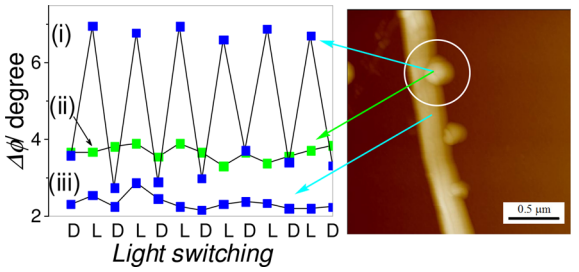

Figure 8. Variations in the phase shift of a magnetized AFM tip 8 nm above the designated nonodot (circled) under illumination at 473 nm (i) and 532 nm (ii), and above the area of 300 nm away from the dot under 473 nm (iii); V_b = 0 V.

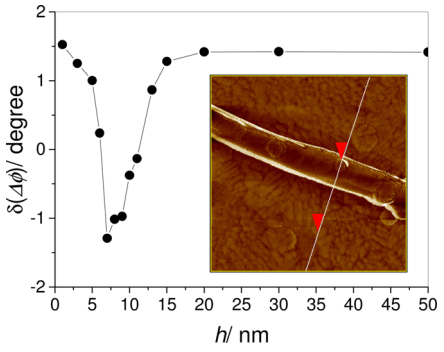

Figure 9. Correlation between the net phase shift of the magnetized tip caused by the designated nanodot (inset) and h.

phase shift against the photocurrent flowing through the Ru@CNT for clues. As shown in Figure 11, the phase shift basically

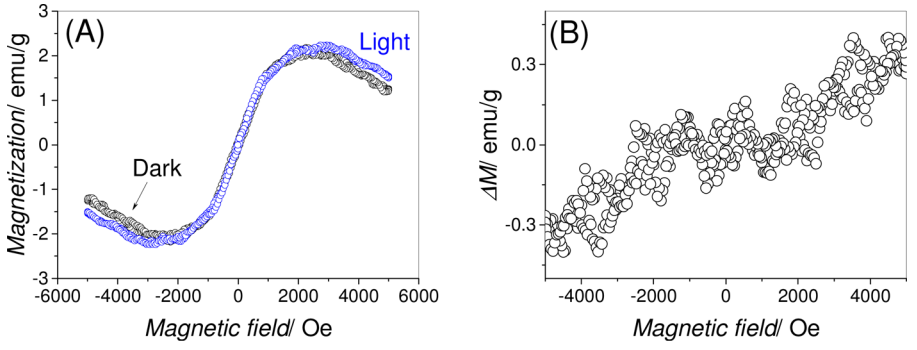

Figure 7. (A) Magnetization curves of the Ru@CNT recorded in the dark and under illumination (473 nm; 27 mW). (B) The net magnetization (ΔM) vs the applied magnetic field.

DOI: 10.1021/acs.jpcc.5b04532
J. Phys. Chem. C 2015, 119, 20673−20680

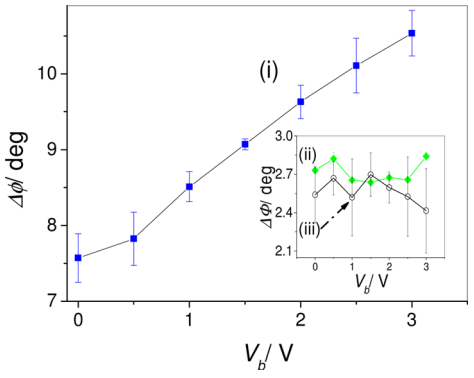

Figure 10. Dependence of the phase shift on the voltage of the electrical bias applied to the Ru@CNT under a constant luminous flux of 473 nm (27 mW, curve (i)), 532 nm (12 mW, curve (ii)), and in the dark (curve (iii)).

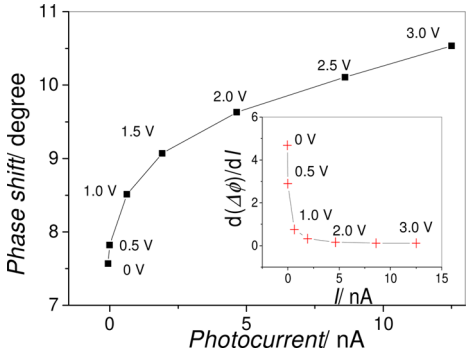

Figure 11. Correlation between the phase shift shown in Figure 10 and the photocurrent (I) flow through the Ru@CNT. Inset shows the relationship between the first derivative of $\Delta\phi$ ($d\Delta\phi/dI$) and I.

increases with the photocurrent, but the increment in terms of the first derivative of $\Delta\phi$ with respect to the current (I) is more significant in the region where charge migration has not virtually started (V_b < 0.5 V, inset). This suggests that the photomagnetism of the Ru@CNT is originating from the unpaired electrons locally confined to the Ru(II)-phen^{2+} nanodots, as illustrated in Scheme 2. The linear relationship observed in the region V_b > 1 V is thus considered to arise from the suppression of the spin annihilation resulting from charge recombination and spin flip due to the virtual migration of charges from the dots to the CNT host. Because of this, the magnetism increases steadily in strength with an increase in the voltage of the applied bias or the current. The k_m of the dot is thus indicated to be V_b-dependent. We also expected that the electrons after being injected into the host could render the entire CNT magnetic. However, we did not observe any photomagnetic signal from the surface of the CNT host even when the applied bias was raised to 3 V. We tentatively attribute this to a limited spin transport length of the electrons while migrating in the CNT host due to charge delocalization.[46] It should also be noted that before and after diazotization, Ru(bpy)$_2$(phen-NH$_2$)$^{2+}$ has no appreciable photoeffects on the MFM tip either in powder form or as a thin film when CNTs are excluded. We attribute the lack of photoresponse to the thermal relaxation due to the disordered distribution of magnetic domains and rapid spin flip, which, in turn, supports the fact that the CNT host is an effective spin-transport medium,[7] that is, it can either promote spin−orbit coupling for the adsorbed sensitizer through the energy states located near the energy gap,[47,48] or enhance the spin of the adsorbates via the Kondo effect.[49] The contrast also highlights that the modification strategy adopted in this work can be applied to regulate the adsorbate so as to be deposited on the CNT host in a symmetrical manner, which is essential for the preparation of magnetic materials. We also attempted to measure the ESR signals for Ru(bpy)$_2$(phen-NH$_2$)$^{2+}$ and its diazotization derivative at low temperature for comparison. However, due to the limitations of the instrumental setup for simultaneous illumination and cooling, this was not possible.

4. CONCLUSIONS

In this work, we demonstrate that Ru(bpy)$_2$(phen-NH$_2$)$^{2+}$ is a useful MLCT complex that can be modified on CNTs in acidic $NaNO_2$ solutions. After the diazotization reaction, the derived radicals form nanodots on the tubes. Similar to their precursor, the nanodots are endowed with the ability to act as photosensitizers and electron acceptors and donors. Because of these properties, the resulting CNTs are capable of transducing optical stimuli (473 nm) into electricity and exhibiting magnetism at ambient conditions. Experiments based on magnetic-mode and conductive-mode AFM techniques indicate that the observed room-temperature magnetism is originating from the unpaired electrons created on the excited nanodots. Ru(bpy)$_2$(phen-NH$_2$)$^{2+}$ does not show a photomagnetic signal either in powder form or as a thin film, which supports that CNTs are an effective spin-transport medium. The photoresponses of the Ru(bpy)$_2$(phen-NH$_2$)$^{2+}$-modified CNTs are highly reproducible, showing that the synthesis strategy proposed in this work is a simple and useful methodology for preparing photomagnetic CNTs, and the modified CNTs are a multifunctional material that has the potential for use in photoelectronics and spintronics research.

■ ASSOCIATED CONTENT

Supporting Information

The Supporting Information is available free of charge on the ACS Publications website at DOI: 10.1021/acs.jpcc.5b04532.

Experimental data and characterizations (PDF)

Demonstration video of the photomagnetic mobility of the Ru@CNT (AVI)

Demonstration video of the photomagnetic mobility of the bare CNTs (AVI)

■ AUTHOR INFORMATION

Corresponding Authors

*E-mail: checmw@ntnu.edu.tw.

*E-mail: jstsay@phy.ntnu.edu.tw.

Notes

The authors declare no competing financial interest.

■ ACKNOWLEDGMENTS

The authors wish to acknowledge Prof. Cheng-Huang Lin for discussions as well as providing the light sources. This work is supported by the National Science Council, Republic of China (Grant No. NSC 102-2113-M-003-002-MY3). J.S.T. acknowledges support from the Ministry of Science and Technology, Taiwan under Contract No. MOST-103-2112-M-003-006.

DOI: 10.1021/acs.jpcc.5b04532
J. Phys. Chem. C 2015, 119, 20673−20680

REFERENCES

(1) Jin, R.; Cao, Y. C.; Hao, E.; Métraux, G. S.; Schatz, G. C.; Mirkin, C. A. Controlling Anisotropic Nanoparticle Growth through Plasmon Excitation. *Nature* **2003**, *425*, 487−490.

(2) Ajayan, P. M.; Tour, J. M. Materials Science: Nanotube Composites. *Nature* **2007**, *447*, 1066−1068.

(3) Dresselhaus, M. S.; Dresselhaus, G.; Avouris, P. E. *Carbon Nanotubes: Synthesis, Structure, Properties, and Applications*; Springer-Verlag: Berlin, 2001.

(4) Bandaru, P. R. Electrical Properties and Applications of Carbon Nanotube Structures. *J. Nanosci. Nanotechnol.* **2007**, *7*, 1239−1267.

(5) Coskun, U. C.; Wei, T.-C.; Vishveshwara, S.; Goldbart, P. M.; Bezryadin, A. *h*/*e* Magnetic Flux Modulation of the Energy Gap in Nanotube Quantum Dots. *Science* **2004**, *304*, 1132−1134.

(6) Ferrier, M.; Ladieu, F.; Ocio, M.; Sacépé, B.; Vaugien, T.; Pichot, V.; Launois, P.; Bouchiat, H. Superconducting Diamagnetic Fluctuations in Ropes of Carbon Nanotubes. *Phys. Rev. B: Condens. Matter Mater. Phys.* **2006**, *73*, 094520.

(7) Zaric, S.; Ostojic, G. N.; Kono, J.; Shaver, J.; Moore, V. C.; Hauge, R. H.; Smalley, R. E.; Xing, W. Estimation of Magnetic Susceptibility Anisotropy of Carbon Nanotubes Using Magneto-photoluminescence. *Nano Lett.* **2004**, *4*, 2219−2221.

(8) Schmid, D. R.; Stiller, P. L.; Strunk, Ch.; Hüttel, A. K. Magnetic Damping of A Carbon Nanotube Nano-Electromechanical Resonator. *New J. Phys.* **2012**, *14*, 083024.

(9) Yoshida, N.; Arie, T.; Akita, S.; Nakayama, Y. Improvement of MFM Tips Using Fe-Alloy-Capped Carbon Nanotubes. *Phys. B* **2002**, *323*, 149−150.

(10) Céspedes, O.; Ferreira, M. S.; Sanvito, S.; Kociak, M.; Coey, J. M. D. Contact Induced Magnetism in Carbon Nanotubes. *J. Phys.: Condens. Matter* **2004**, *16*, L155−L161.

(11) Ferreira, M. S.; Sanvito, S. Contact-Induced Spin Polarization in Carbon Nanotubes. *Phys. Rev. B: Condens. Matter Mater. Phys.* **2004**, *69*, 035407.

(12) Karousis, N.; Tagmatarchis, N. Current Progress on the Chemical Modification of Carbon Nanotubes. *Chem. Rev.* **2010**, *110*, 5366−5397.

(13) Masotti, A.; Caporali, A. Preparation of Magnetic Carbon Nanotubes (Mag-CNTs) for Biomedical and Biotechnological Applications. *Int. J. Mol. Sci.* **2013**, *14*, 24619−24642.

(14) Niklas, J.; Holt, J. M.; Mistry, K.; Rumbles, G.; Blackburn, J. L.; Poluektov, O. G. Charge Separation in P3HT:SWCNT Blends Studied by EPR: Spin Signature of the Photoinduced Charged State in SWCNT. *J. Phys. Chem. Lett.* **2014**, *5*, 601−606.

(15) Teale, R. W.; Temple, D. W. Photomagnetic Anneal, A new Magneto-Optic Effect, in Si-Doped Yittrium Iron Garnet. *Phys. Rev. Lett.* **1967**, *19*, 904−905.

(16) Ratera, I.; Veciana, J. Photomagnetism in Molecular Materials. In *Encyclopedia of Supramolecular Chemistry*; Atwood, J. L., Steed, J. W., Wallace, K. J., Eds.; Taylor & Francis: New York, 2012.

(17) Shimamoto, N.; Ohkoshi, S.; Sato, O.; Hashimoto, K. One-Shot-Laser-Pulse-Induced Cooperative Charge Transfer Accompanied by Spin Transition in A Co-Fe Prussian Blue Analog at Room Temperature. *Chem. Lett.* **2002**, *31*, 486−487.

(18) Liu, H. W.; Matsuda, K.; Gu, Z. Z.; Takahashi, K.; Cui, A. L.; Nakajima, R.; Fujishima, A.; Sato, O. Reversible Valence Tautomerism Induced by A Single-Shot Laser Pulse in A Cobalt-Iron Prussian Blue Analog. *Phys. Rev. Lett.* **2003**, *90*, 167403.

(19) Herrera, J. M.; Marvaud, V.; Verdaguer, M.; Marrot, J.; Kalisz, M.; Mathonière, C. Reversible Photoinduced Magnetic Properties in the Heptanuclear Complex $[Mo^{IV}(CN)_2(CN\text{-}CuL)_6]^{8+}$: A Photomagnetic High-Spin Molecule. *Angew. Chem., Int. Ed.* **2004**, *43*, 5468−5471.

(20) Kimel, A. V.; Kirilyuk, A.; Usachev, P. A.; Pisarev, R. V.; Balbashov, A. M. Rasing, Th. Ultrafast Non-Thermal Control of Magnetization by Instantaneous Photomagnetic Pulses. *Nature* **2005**, *435*, 655−657.

(21) Létard, J.-F. Photomagnetism of Iron(II) Spin Crossover Complexes−the *T*(LIESST) Approach. *J. Mater. Chem.* **2006**, *16*, 2550−2559.

(22) Cobo, S.; Ostrovskii, D.; Bonhommeau, S.; Vendier, L.; Molnár, G.; Salmon, L.; Tanaka, K.; Bousseksou, A. Single-Laser-Shot-Induced Complete Bidirectional Spin Transition at Room Temperature in Single Crystals of $(Fe^{II}(pyrazine)(Pt(CN)_4))$. *J. Am. Chem. Soc.* **2008**, *130*, 9019−9024.

(23) Bozdag, K. D.; Yoo, J.-W.; Raju, N. P.; McConnell, A. C.; Miller, J. S.; Epstein, A. J. Optical Control of Magnetization in A Room-Temperature Magnet: V-Cr Prussian Blue Analog. *Phys. Rev. B: Condens. Matter Mater. Phys.* **2010**, *82*, 094449.

(24) Cafun, J.-D.; Lejeune, J.; Baudelet, F.; Dumas, P.; Itié, J.-P.; Bleuzen, A. Room-Temperature Photoinduced Electron Transfer in A Prussian Blue Analogue under Hydrostatic Pressure. *Angew. Chem., Int. Ed.* **2012**, *51*, 9146−9148.

(25) Szaciłowski, K.; Macyk, W.; Drzewiecka-Matuszek, A.; Brindell, M.; Stochel, G. Bioinorganic Photochemistry: Frontiers and Mechanisms. *Chem. Rev.* **2005**, *105*, 2647−2694.

(26) Ellis, C. D.; Margerum, L. D.; Murray, R. W.; Meyer, T. J. Oxidative Electropolymerization of Polypyridyl Complexes of Ruthenium. *Inorg. Chem.* **1983**, *22*, 1283−1291.

(27) Wolf, S. A.; Awschalom, D. D.; Buhrman, R. A.; Daughton, J. M.; von Molnár, S.; Roukes, M. L.; Chtchelkanova, A. Y.; Treger, D. M. Pintronics: A Spin-Based Electronics Vision for the Future. *Science* **2001**, *294*, 1488−1495.

(28) Dyke, C. A.; Tour, J. M. Solvent-Free Functionalization of Carbon Nanotubes. *J. Am. Chem. Soc.* **2003**, *125*, 1156−1157.

(29) Balasubramanian, K.; Friedrich, M.; Jiang, C.; Fan, Y.; Mews, A.; Burghard, M.; Kern, K. Electrical Transport and Confocal Raman Studies of Electrochemically Modified Individual Carbon Nanotubes. *Adv. Mater.* **2003**, *15*, 1515−1518.

(30) Maultzsch, J.; Reich, S.; Thomsen, C.; Webster, S.; Czerw, R.; Carroll, D. L.; Vieira, S. M. C.; Birkett, P. R.; Rego, C. A. Raman Characterization of Boron-Doped Multiwalled Carbon Nanotubes. *Appl. Phys. Lett.* **2002**, *81*, 2647−2649.

(31) Agnès, C.; Arnault, J.-C.; Omnès, F.; Jousselme, B.; Billon, M.; Bidan, G.; Mailley, P. XPS Study of Ruthenium *tris*-Bipyridine Electrografted from Diazonium Salt Derivative on Microcrystalline Boron Doped Diamond. *Phys. Chem. Chem. Phys.* **2009**, *11*, 11647−11654.

(32) Mikroyannidis, J.; Papagelis, K.; Fakis, M.; Tasis, D. Carbon Nanotube−Fluorenevinylene Hybrids: Synthesis and Photophysical Properties. *Chem. Phys. Lett.* **2009**, *483*, 241−246.

(33) Englman, R.; Jortner, J. The Energy Gap Law for Radiationless Transitions in Large Molecules. *Mol. Phys.* **1970**, *18*, 145−164.

(34) Piao, Y. M.; Meany, B.; Powell, L. R.; Valley, N.; Kwon, H.; Schatz, G. C.; Wang, Y. Brightening of Carbon Nanotube Photoluminescence through the Incorporation of sp^3 Defects. *Nat. Chem.* **2013**, *5*, 840−845.

(35) Chou, P.-T.; Chi, Y.; Chung, M.-W.; Lin, C.-C. Harvesting Luminescence via Harnessing the Photophysical Properties of Transition Metal Complexes. *Coord. Chem. Rev.* **2011**, *255*, 2653−2665.

(36) Felder, D.; Nierengarten, J.-F.; Barigelletti, F.; Ventura, B.; Armaroli, N. Highly Luminescent Cu(I)−Phenanthroline Complexes in Rigid Matrix and Temperature Dependence of the Photophysical Properties. *J. Am. Chem. Soc.* **2001**, *123*, 6291−6299.

(37) Ito, O.; D'Souza, F. Recent Advances in Photoinduced Electron Transfer Processes of Fullerene-Based Molecular Assemblies and Nanocomposites. *Molecules* **2012**, *17*, 5816−5835.

(38) McCarthy, M. A.; Liu, B.; Donoghue, E. P.; Kravchenko, I.; Kim, D. Y.; So, F.; Rinzler, A. G. Low-Voltage, Low-Power, Organic Light-Emitting Transistors for Active Matrix Displays. *Science* **2011**, *332*, 570−573.

(39) Mohapatra, S.; Kumar, R. K.; Maji, T. K. Green Synthesis of Catalytic and Ferromagnetic Gold Nanoparticles. *Chem. Phys. Lett.* **2011**, *508*, 76−79.

DOI: 10.1021/acs.jpcc.5b04532
J. Phys. Chem. C 2015, 119, 20673−20680

(40) Khavrus, V. O.; Ibrahim, E. M. M.; Bachmatiuk, A.; Rümmeli, M. H.; Wolter, A. U. B.; Hampel, S.; Leonhardt, A. High-Pressure Catalytic Chemical Vapor Deposition of Ferromagnetic Ruthenium-Containing Carbon Nanostructures. *J. Nanopart. Res.* **2012**, *14*, 914.
(41) Garitaonandia, J. S.; Insausti, M.; Goikolea, E.; Suzuki, M.; Cashion, J. D.; Kawamura, N.; Ohsawa, H.; de Muro, I. G.; Suzuki, K.; Plazaola, F.; et al. Chemically Induced Permanent Magnetism in Au, Ag, and Cu Nanoparticles: Localization of the Magnetism by Element Selective Techniques. *Nano Lett.* **2008**, *8*, 661−667.
(42) Moocarme, M.; Domínguez-Juárez, J. L.; Vuong, L. T. Ultralow-Intensity Magneto-Optical and Mechanical Effects in Metal Nanocolloids. *Nano Lett.* **2014**, *14*, 1178−1183.
(43) Sakamoto, Y.; Oba, Y.; Maki, H.; Suda, M.; Einaga, Y.; Sato, T.; Mizumaki, M.; Kawamura, N.; Suzuki, M. Ferromagnetism of Pt Nanoparticles Induced by Surface Chemisorption. *Phys. Rev. B: Condens. Matter Mater. Phys.* **2011**, *83*, 104420.
(44) Chen, Y.-T.; Xie, S. M.; Jheng, H. Y. The Low-Frequency Alternative-Current Magnetic Susceptibility and Electrical Properties of Si(100)/$Fe_{40}Pd_{40}B_{20}$(X Å)/ZnO(500 Å) and Si(100)/ZnO(500 Å)/$Fe_{40}Pd_{40}B_{20}$(Y Å) Systems. *J. Appl. Phys.* **2013**, *113*, 17B303.
(45) Gomez, R. D.; Pak, A. O.; Anderson, A. J.; Burke, E. R.; Leyendecker, A. J.; Mayergoyz, I. D. Quantification of Magnetic Force Microscopy Images Using Combined Electrostatic and Magnetostatic Imaging. *J. Appl. Phys.* **1998**, *83*, 6226−6228.
(46) Zhang, X.; Mizukami, S.; Kubota, T.; Ma, Q.; Oogane, M.; Naganuma, H.; Ando, Y.; Miyazaki, T. Observation of A Large Spin-Dependent Transport Length in Organic Spin Valves at Room Temperature. *Nat. Commun.* **2013**, *4*, 1392.
(47) Minot, E. D.; Yaish, Y.; Sazonova, V.; McEuen, P. L. Determination of Electron Orbital Magnetic Moments in Carbon Nanotubes. *Nature* **2004**, *428*, 536−539.
(48) Ramirez, A. P.; Haddon, R. C.; Zhou, O.; Fleming, R. M.; Zhang, J.; McClure, S. M.; Smalley, R. E. Magnetic Susceptibility of Molecular Carbon: Nanotubes and Fullerite. *Science* **1994**, *265*, 84−86.
(49) Odom, T. W.; Huang, J.-L.; Cheung, C. L.; Lieber, C. M. Magnetic Clusters on Single-Walled Carbon Nanotubes: the Kondo Effect in A One-Dimensional Host. *Science* **2000**, *290*, 1549−1552.

DOI: 10.1021/acs.jpcc.5b04532
J. Phys. Chem. C 2015, 119, 20673−20680